A new gigantic titanosaurian sauropod from the early Late Cretaceous of Patagonia (Neuquén Province, Argentina)

MARÍA EDITH SIMÓN and LEONARDO SALGADO

A new gigantic titanosaur *Bustingorrytitan shiva* gen. et sp. nov. is described. The four specimens upon which this species is erected come from Neuquén Province, Argentina, from levels of the Huincul Formation (Cenomanian). *Bustingorrytitan shiva* gen. et sp. nov. exhibits some autapomorphic characters such as posterior dorsal vertebrae with spinodiapophyseal laminae bifurcated in two, very well developed anterior and posterior spinodiapophyseal lamina rami, which limit a deep, vertical, socket-like fossa; posterior dorsal neural arches with forked centropostzygapophyseal laminae; hyposphene in anterior caudal vertebrae; humerus with deltopectoral crest strongly expanded distally; and femur with a low longitudinal crest on the lateromedial half of the anterior face, bifurcated in two minor crests, which are directed to their respective condyles. The phylogenetic analysis performed recovers *B. shiva* gen. et sp. nov. as a lithostrotian, the sister taxon of Saltasauridae. The estimated body mass is 67.297 metric tons (with a standard error of ±17.228), which makes *B. shiva* gen. et sp. nov. one of the largest sauropods ever recorded. The record of this new sauropod corroborates the idea that gigantism (evolution of forms over the 50 metric tons) would have evolved many times within Eutitanosauria.

Key words: Dinosauria, Sauropoda, Titanosauria, Cretaceous, Neuquén, Patagonia.

María Edith Simón [paleoedith@gmail.com; ORCID: https://orcid.org/0009-0007-0735-5567], Agrimensor Moreno 911, Barrio Gamma, Ciudad de Neuquén (8300), 8300 Neuquén, Argentina.
Leonardo Salgado [lsalgado@unrn.edu.ar; ORCID: https://orcid.org/0000-0003-3066-0870], Instituto de Investigación en Paleobiología y Geología, Universidad Nacional de Río Negro-Conicet, Av. Julio A. Roca 1242, 8322 General Roca, Río Negro, Argentina.

Introduction

Titanosaurs include the largest terrestrial animals that ever lived. Five species, four of which inhabited Patagonia, would have reached body masses of ~50 tons or more: *Patagotitan mayorum* (Cerro Barcino Formation, latest Albian), *Argentinosaurus huinculensis* (Huincul Formation, Cenomanian–Turonian), *Notocolossus gonzalezparejasi* (Plottier Formation, Santonian), not from Patagonia but from the Neuquén Basin, Puertasaurus reuili (Cerro Fortaleza Formation, Campanian), and *Dreadnoughtus schrani* (Cerro Fortaleza Formation, Campanian) (Carballido et al. 2017; Bonaparte and Coria 1993; González Riga et al. 2016; Novas et al. 2005; Lacovara et al. 2014). However, only one of these, *D. schrani*, preserves a humerus and femur from a single individual, with the possibility to estimate the body mass by means of scaling equations, which are robust predictors of body mass in quadrupedal tetrapods (Anderson 1985; Campione and Evans 2012). In fact, the holotype of *D. schrani* (MPM-PV 1156), which includes at least 70% of the whole skeleton, preserves a humerus and femur (Lacovara et al. 2014). The *Patagotitan mayorum* holotype (MPEF-PV 3400) and one of the paratypic specimens (MPEF-PV 3499) preserve a femur but not a humerus, which is known from additional paratypes (MPEF-PV 3394, 3395, 3396, 3397, 3375), which in turn do not preserve femora (even thus, its body mass was estimated based on these two bones from different specimens). The *Futalognkosaurus dukei* holotype preserves most of the vertebral column and a pelvis. The original description of this sauropod (Calvo et al. 2007) did not include limb bones. Although later Jorge Orlando Calvo reported the finding of a humerus (of 1560 mm of length) and a femur (of 1980 mm of length) at the site
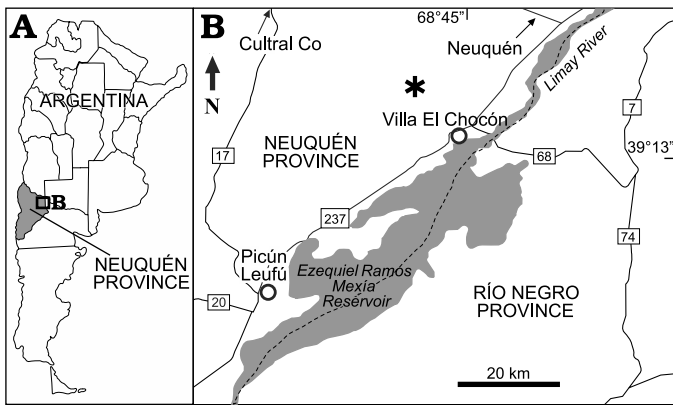
Fig. 1. **A**. General location map of Neuquén Province. **B**. Location of the fossiliferous site (asterisk) in the surroundings of Villa El Chocón, Neuquén Province (modified from Otero et al. 2011).

of the type material (Calvo 2014), these bones were never formally included in the holotype of *Futalognkosaurus dukei*, and neither properly described nor figured.

For this reason these are not taken into acccount in this list. The other gigantic titanosaurs (*Argentinosaurus huinculensis*, *Puertasaurus reuili*) are quite incomplete, as is the skeleton recently published by Otero et al. (2021), which comes from 100 km north-northeast of Zapala City (Neuquén Province) and from the upper part of the Candeleros Formation, Upper Cretaceous (Cenomanian).

Here, we describe a new gigantic titanosaur from Patagonia (Neuquén Province, Argentina; Fig. 1). The material upon which we establish the new species was collected from the base of the Huincul Formation (upper Cenomanian) (Fig. 2) and consists of a relatively complete skeleton, and three other incomplete specimens (Fig. 3). The first gigantic titanosaur to be discovered (in 1989), *Argentinosaurus huinculensis* (Bonaparte and Coria 1993), comes from the upper levels of this unit, but at a distance of 50 km to the northwest.

Institutional abbreviations.—MMCH-Pv, paleovertebrate collection, Museo Municipal de Villa El Chocón "Ernesto Bachmann", Neuquén, Argentina; MPEF-Pv, paleovertebrate collection, Museo Paleontológico "Egidio Feruglio", Trelew, Argentina.

Other abbreviations.—aspdl, anterior spinodiapophyseal lamina; cpaf, centroparapophyseal fossa; BM, body mass; cpol, centropostzygapophyseal lamina; cprl, centroprezygapophyseal lamina; cprl, centroprezygapophyseal lamina; prdl, prezygodiapophyseal lamina; podl, postzygodiapophyseal lamina; pacdf, parapophyseal centrodiapophyseal fossa; cpol, centropostzygapophyseal lamina; pocdf, postzygapophyseal centrodiapophyseal fossa; pspdl, posterior spinodiapophyseal laminae; posdf, postzygapophyseal spinodiapophyseal fossa; PPE, percent prediction error; prsl, prespinal lamina; lspol, lateral spinopostzygapophyseal lamina; pspdl, posterior spinodiapophyseal lamina, spol, spinopostzygapophyseal lamina; tpol, intrapostzygapophyseal lamina; tprl, intraprezygapophyseal lamina.
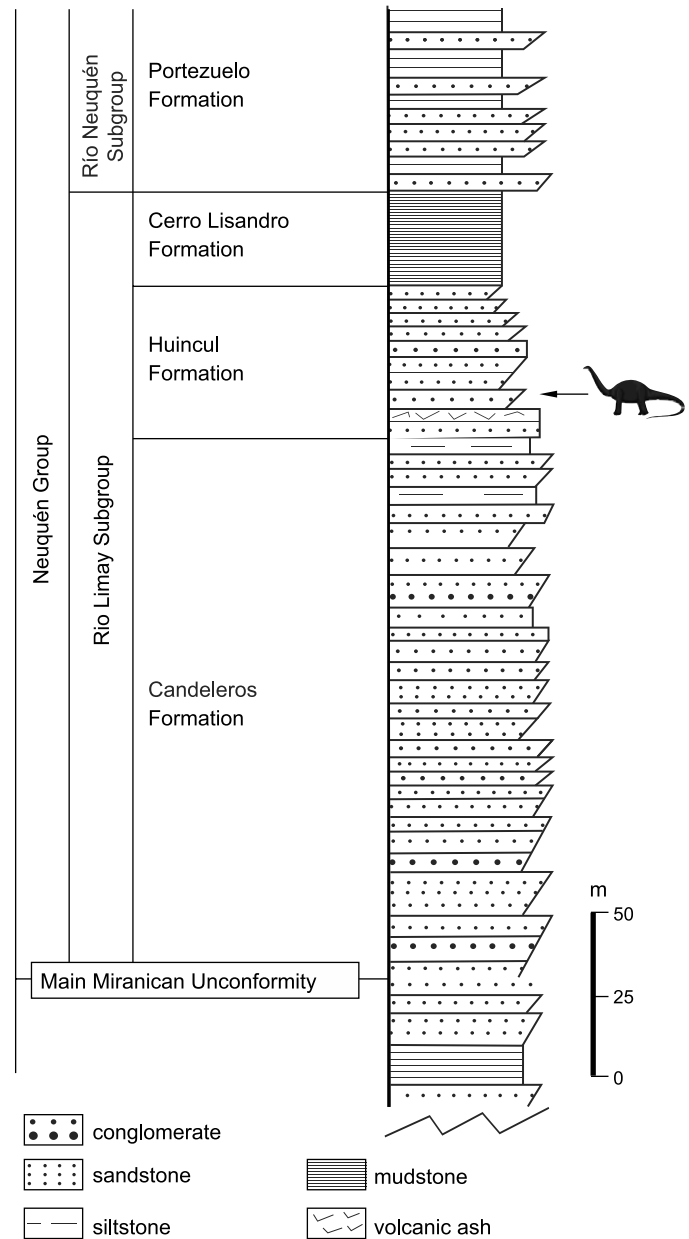

Fig. 2. Simplified section of the site showing the stratigraphical position of *Bustingorrytitan shiva* gen. et sp. nov. (modified from Otero et al. 2011).

Nomenclatural acts.—This published work and the nomenclatural acts it contains have been registered in ZooBank: urn:lsid:zoobank.org:pub:93EC5275-CF4E-4709-85CF-3853DEABD175.

Systematic palaeontology

Dinosauria Owen, 1842

Saurischia Seeley, 1888

Sauropoda Marsh, 1878

Titanosauriformes Salgado, Coria, and Calvo, 1997

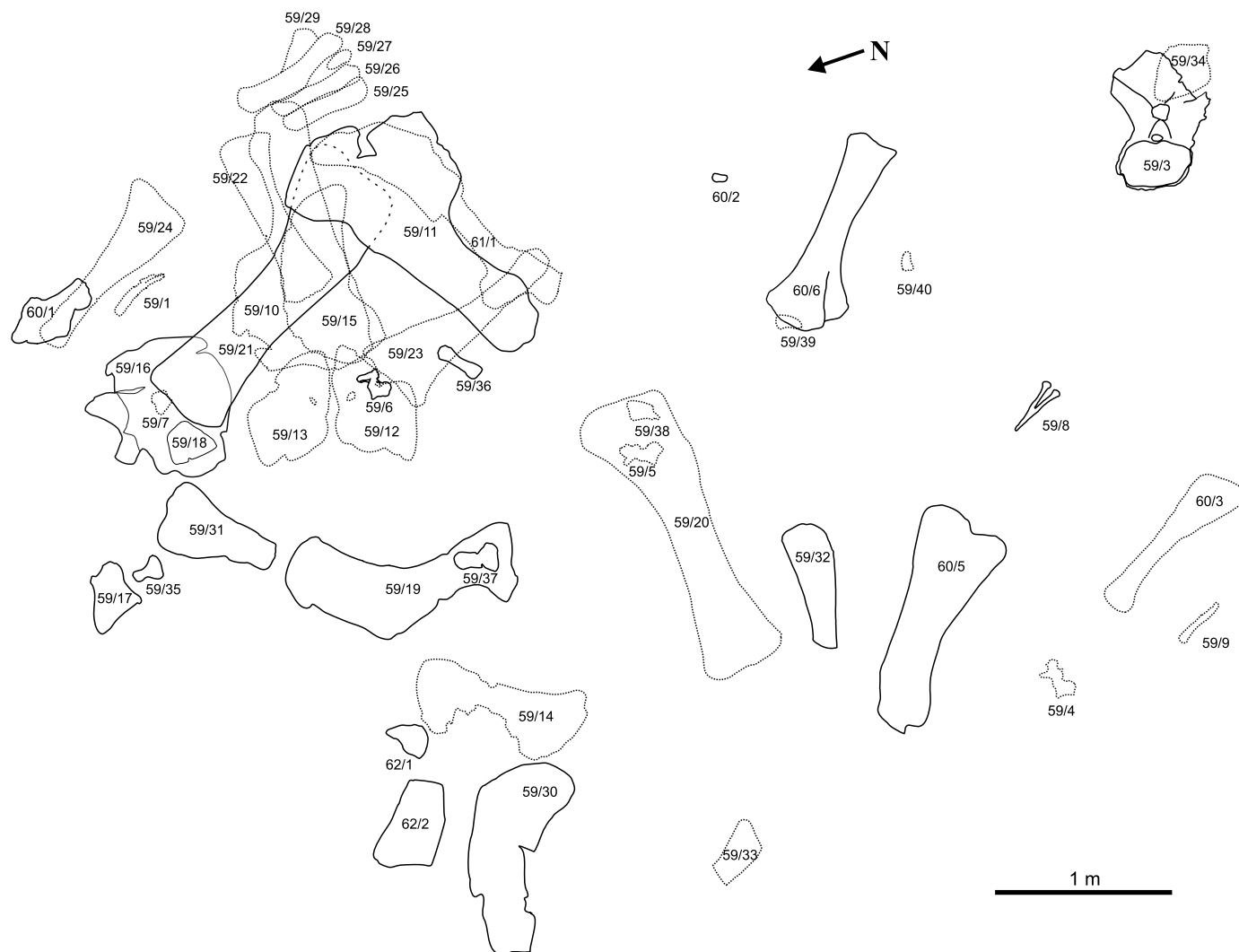Titanosauria Bonaparte and Coria, 1993

Fig. 3. Spatial distribution of skeletal elements of the titanosaurian sauropod *Bustingorrytitan shiva* gen. et sp. nov. from "Bustingorry II" site, Neuquén Province, Argentina, upper Cenomanian. Numbers correspond to MMCH-Pv specimens. The solid lines correspond to the materials extracted in the first field works February 1–10, 2001 (when the bones overlap in some sector, it is continued with stippled lines). The materials extracted during the second and third field works (November 30–December 9, 2001, and December 15–22, 2001), are indicated by dotted lines.

Lithostrotia Upchurch, Barrett, and Dodson, 2004

Genus *Bustingorrytitan* nov.

Zoobank LSID: zoobank.org:act:BB436E66-7433-4319-96E7-ED690 DFE1088

Type species: *Bustingorrytitan shiva* sp. nov.; see below.

Etymology: In gratitude to Manuel Bustingorry, owner of the land in the surroundings of Villa El Chocón where the remains were found, and for his support during the execution of the fieldworks; and from Greek *titan*, giant god; for the gigantism achieved by this species.

Diagnosis.—As for the type species.

Bustingorrytitan shiva sp. nov.

Figs. 4–6.

Zoobank LSID: zoobank.org:act:F140E7D1-D8BC-47A8-BC49-423E 9763A7AE

Etymology: From *Shiva*, supreme deity of Shivaism, branch of Hinduism, who destroys and transforms the Universe, in allusion to the faunal turnover that occurred in the middle of the Cretaceous period, towards the Cenomanian/Turonian boundary.

Type material: Holotype, MMCH-Pv 59/1–40: partial skeleton composed of right dentary (MMCH-Pv 59/1), tooth fragment (MMCH-Pv 59/2), sixth? or seventh? dorsal vertebra (MMCH-Pv 59/3), two anterior caudal vertebrae (MMCH-Pv 59/4 y MMCH-Pv 59/5), mid caudal vertebra (MMCH-Pv 59/6), mid-posterior caudal vertebra (MMCH-Pv 59/7); two haemal arches (MMCH-Pv 59/8 and MMCH-Pv 59/9), right and left scapulae (MMCH-Pv 59/10 and MMCH-Pv 59/11), right and left coracoids (MMCH-Pv 59/12 and MMCH-Pv 59/13), right and left sternal plates (MMCH-Pv 59/14 and MMCH-Pv 59/15), left ilium (MMCH-Pv 59/16) and right and left pubic peduncles of the ilium (MMCH-Pv 59/17 and MMCH-Pv 59/18), right pubis (MMCH-Pv 59/19), right and left humeri (MMCH-Pv 59/20 and MMCH-Pv 59/21), right radius (MMCH-Pv 59/22), right and left ulnae (MMCH-Pv 59/23 and MMCH-Pv 59/24), five right metacarpals I, II, III, IV and V (MMCH-Pv 59/25, MMCH-Pv 59/26, MMCH-Pv 59/27, MMCH-Pv 59/28 and MMCH-Pv 59/29), right femur (MMCH-Pv 59/30), right tibia (MMCH-Pv 59/31), right and left fibulae (MMCH-Pv 59/32 and MMCH-Pv 59/33), left astragalus (MMCH-Pv 59/34), three metatarsals I, IV?, V (MMCH-Pv 59/35, MMCH-Pv 59/36, MMCH-Pv

59/37) and three right ungual phalanges I, II, and III (MMCH-Pv 59/38, MMCH-Pv 59/39 and MMCH-Pv 59/40). Paratype, MMCH-Pv 60/1–6, partial skeleton smaller than the holotype composed of a mid to posterior cervical vertebra (MMCH-Pv 60/1), a posterior caudal vertebra (MMCH-Pv 60/2), a right ulna (MMCH-Pv 60/3), a metacarpal III (MMCH-Pv 60/4), a right femur (MMCH-Pv 60/5), and a left tibia (MMCH-Pv 60/6). All from the type locality and horizon.

Type locality: "Bustingorry II" site (S 39°12'30"; W 68°48'53"), Neuquén Province, Patagonia, Argentina.

Type horizon: Huincul Formation, Neuquén Group, Upper Cretaceous, upper Cenomanian (Legarreta and Gulisano, 1989; Leanza, 1999) (Fig. 1). The fossiliferous level is 60 m above the fossiliferous level of "La Antena" Quarry, where the remains of *Choconsaurus baileywillisi* Simón, Salgado, and Calvo, 2018, were discovered near the contact with the underlying Candeleros Formation (Fig. 2).

Material.—At least four individuals have been recognized based on the association of bones in the quarry, and the comparison of their sizes: MMCH-Pv 59/1–40 (holotype), MMCH-Pv 60/1–6 (paratype), MMCH-Pv 61, 62. MMCH-Pv 61, specimen even smaller than the paratype composed of only by the left femur (MMCH-Pv 61/1). MMCH-Pv 62, specimen larger than the holotype integrated by the right femur (MMCH-Pv 62/1), left tibia (MMCH-Pv 62/2) and left astragalus (MMCH-Pv 62/3). The repeated bones (posterior caudal vertebrae, ulnae, metacarpals III, femora, tibiae, astragali) are identical in the four individuals, the reason why we interpret that all the material belongs to the same species. Moreover, the ulna of the paratype (MMCH-Pv 60/3) exhibits the autapomorphy recognized on the holotype (MMCH-Pv 59/23 and MMCH-Pv 59/24).

Diagnosis.—*Bustingorrytitan shiva* gen. et sp. nov. is characterized by the following autapomorphies (those indicated by an asterisk are those autapomorphies recovered by the phylogenetic analysis): *ventral surface of the cervical centrum concave transversely; *pleurocoels absent in cervical centrum; *slightly opisthocoelous posterior dorsal vertebrae; *pleurocoel with angular dorsal margin in middle to posterior dorsal vertebrae; *dorsal margin of pleurocoels at the level of or higher than the dorsal margin of the centrum in posterior dorsal vertebrae; *neural spine of middle to posterior dorsal vertebrae with subparallel lateral margins in anterior posterior view; posterior dorsal vertebrae with very developed anterior (aspdl) and posterior (pspdl) spinodiapophyseal laminae, limiting a deep, vertical, socket-like fossa; posterior dorsal neural arches with forked centropostzygapophyseal laminae (cpol); *prespinal lamina (prsl) rough and wide, extended through almost all the neural spine, in dorsal vertebrae; *presence of a single lamina (the single tpol) supporting the hyposphene or postzygapophysis from below in mid and posterior dorsal vertebrae; *absence of lateral spinopostzygapophyseal lamina (lspol) in middle and posterior dorsal neural spine; *height of neural arch below the postzygapophyses (pedicel) subequal to or greater than height of centrum in mid and posterior dorsal vertebrae; *solid, not pneumatized, neural arches in anterior caudal vertebrae; *anterior caudal vertebrae with spinoprezygapophyseal laminae ventral and medially placed, usu-

ally described as bifurcated prsl; *anterior caudal vertebrae with spol poorly developed causing the articular facet of the postzygapophysis to project slightly from the midline; hyposphene in anterior caudal vertebrae; *middle caudal centra with flat ventral margin; *prezygapophyses of mid caudal vertebrae anterodorsally oriented (around 45°); *well developed acromion process of scapula; *acromial process placed at nearly midpoint of the scapular body; *scapular acromion at least 1/2 of scapular length; *glenoid scapular orientated relatively flat or laterally facing; *dorsal margin of the coracoid lies, in lateral view, below the level of the scapular proximal expansion and separated from the latter by a V-shaped notch; *humerus gracile (RI less than 0.27); *radial condyle of humerus divided on anterior face by a notch; humerus with deltopectoral crest strongly expanded distally; *ulnar olecranon process rudimentary; *transverse axis of the distal condyle of metacarpal I beveled approximately 20° respect to axis of shaft; *proximal symphysis of the pubis forming a marked ventromedially directed process; femur with a low longitudinal crest on the lateromedial half of the anterior face, bifurcated in two lesser crests, each of which is directed to one of the condyles; *distal breadth of tibia approximately 125% its midshaft breadth; *minimum transverse shaft diameters of metatarsals III and IV subequal to that of metatarsals I or II; *metatarsal V shorter than metatarsal IV.

Stratigraphic and geographic range.—Huincul Formation (upper Cenomanian), "Bustingorry II" site, Villa El Chocón, Neuquén Province, Argentina.

Description

Cranial skeleton.—*Dentary*: The right dentary MMCH-Pv 59/1 is low and long, with its height virtually invariable throughout its length; at least, this is what is seen in its best-preserved portion. The dorsal process originates posteriorly to the 11th alveolous; at this point, the dentary curves slightly medially (Fig. 4A).

In medial view (Fig. 4A₁), part of the splenial furrow is visible; it extends approximately from the position of the ninth alveolous up to the posterior end of the preserved portion of the bone.

The dentary has at least 12 alveoli with 10 in situ teeth, of which those corresponding to the 7th and 10th alveoli are the only visible in lateral view (Fig. 4A₁). Alveoli 1 and 2 house unerupted replacement teeth, whereas other alveoli (3, 5, 9 and 12) house only the bases of broken teeth. Teeth are oriented perpendicularly to the alveolar margin, as in most titanosaurs (Calvo 1994), and have an elliptical cross-section. As far as can be seen, the teeth are compressed-cone-chisel-like, although this cannot be established with certainty due to the poor preservation both of the isolated fragmentary tooth (MMCH-Pv 59/2) and the implanted teeth. For the same reason, their slenderness index cannot be established, as well as whether or not they had carinae on their mesial/distal margins. None of the 10 preserved teeth shows wear facets.
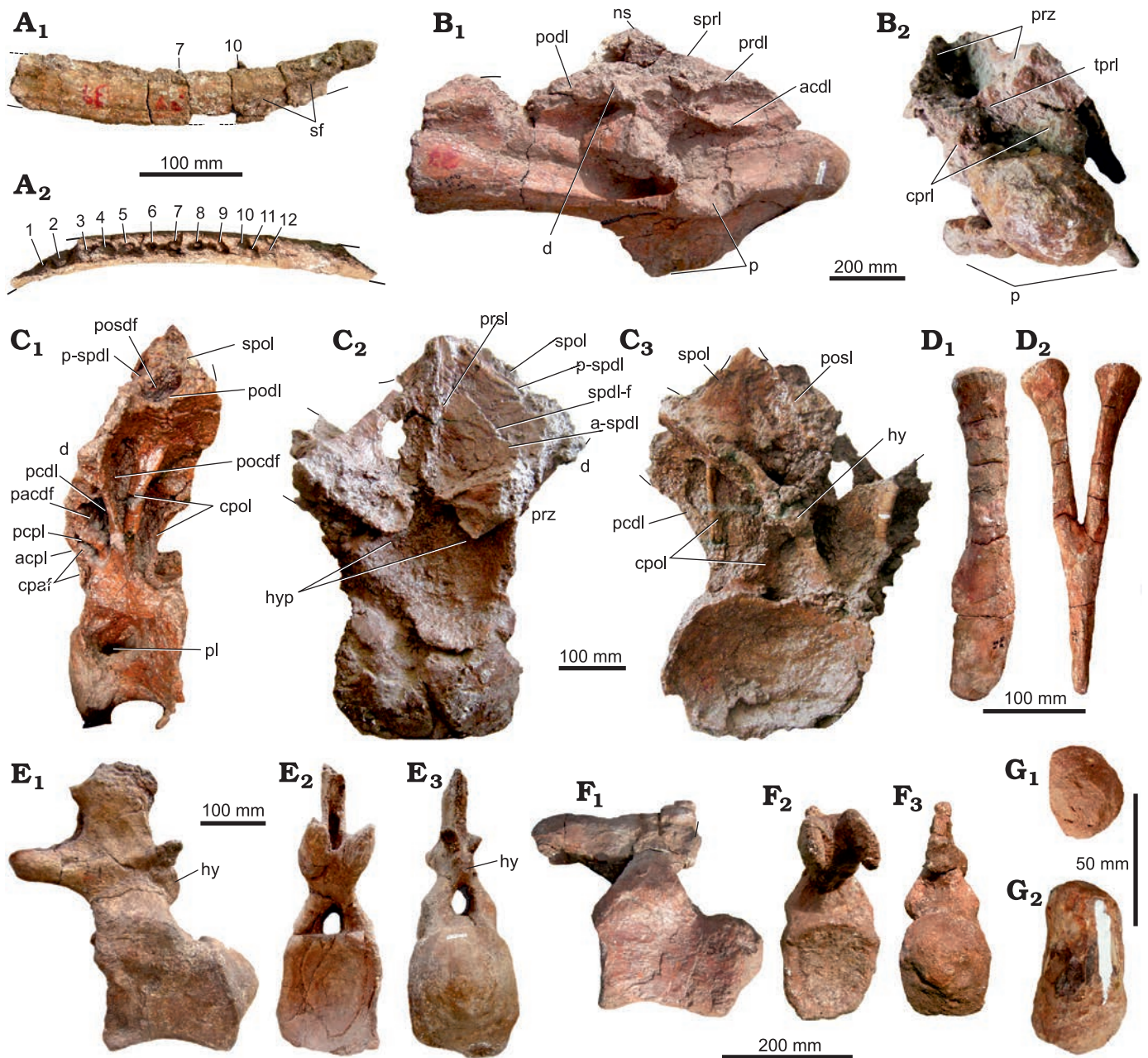
Fig. 4. Axial skeleton of the titanosaurian sauropod *Bustingorrytitan shiva* gen. et sp. nov. from "Bustingorry II" site, Neuquén Province, Argentina, upper Cenomanian. **A**. Right dentary (holotype, MMCH-Pv 59/1) in medial (A_1) and dorsal (A_2) views (numbers indicate alveoli with partial teeth). **B**. Mid to posterior cervical vertebra (paratype, MMCH-Pv 60/1) in right ventro-lateral (B_1) and anterior (B_2) views. **C**. Sixth? or seventh? dorsal vertebra (holotype, MMCH-Pv 59/3) in left lateral (C_1), anterior (C_2), and posterior (C_3) views. **D**. Haemal arch (holotype, MMCH-Pv 59/8) in right lateral (D_1) and anterior (D_2) views. **E**. Anterior caudal vertebra (holotype, MMCH-Pv 59/4) in left lateral (E_1), anterior (E_2), and posterior (E_3) views. **F**. Mid-caudal vertebra (holotype, MMCH-Pv 59/6) in left lateral (F_1), anterior (F_2), and posterior (F_3) views. **G**. Posterior caudal vertebra (paratype, MMCH-Pv 60/2) in anterior (G_1) and left lateral (G_2) views. Abbreviations: acdl, anterior centrodiapophyseal lamina; acpl, anterior centroparapophyseal lamina; a-spdl, anterior ramus of the spinodiapophyseal lamina; cpaf, centroparapophyseal fossa; cpol, centropostzygapophyseal lamina; cprl: centroprezygapophyseal lamina; d, diapophysis; hy, hyposphene; hyp, hypantrum; ns, neural spine; p, parapophysis; pacdf, parapophyseal centrodiapophyseal fossa; pcdl, posterior centrodiapophyseal lamina; pcpl, posterior centroparapophyseal lamina; pl, pleurocoel; pocdf, postzygapophyseal centrodiapophyseal fossa; podl, postzygodiapophyseal lamina; posdf, postzygapophyseal spinodiapophyseal fossa; prdl, prezygodiapophyseal lamina; prsl, prespinal lamina; prz, prezygapophysis; p-spdl, posterior ramus of the spinodiapophyseal lamina; sf, splenial furrow; spdl-f, spinodiapophyseal lamina fossa; spol, spinopostzygapophyseal lamina; spol, spinopostzygapophyseal lamina; sprl, spinoprezygapophyseal lamina; tprl, intraprezygapophyseal lamina.

Axial skeleton.—*Cervical vertebra*: MMCH-Pv 60/1, the only known cervical vertebra of *Bustingorrytitan shiva* gen. et sp. nov. is probably a middle to posterior cervical and is part of the paratype. It is rather complete (it only lacks the

tip of the neural spine, the right diapophysis and both postzygapophyses) though deformed, in spite of which it is visibly opisthocoelic (Fig. 4B). The centrum length (counting the condyle) is 540 mm, and its average Elongation Index

is 3.91 (centrum length excluding the condyle = 47/average between height and width of the posterior articulation = 12). Its lateral face presents a longitudinal, deep depression, without a pneumatic foramen or pleurocoel on its bottom, differing in this with the posterior cervical vertebrae of *P. mayorum* (Carballido et al. 2017) and the 3rd cervical of *Nullotitan glaciaris* (Novas et al. 2019: fig. 15). Internally, it is not possible to observe the pattern of pneumaticity of the centrum. The ventral face is relatively flat, both transversely and anteroposteriorly (Fig. 4B$_1$).

The diapophyses are placed at nearly the middle of the centrum. The parapophysis is very robust, not as tabular as in the ninth cervical of *Puertasaurus reuili* (Novas et al. 2005: fig. 1A–D) and the third cervical of *Nullotitan glaciaris* (Novas et al. 2019: fig. 15). The spinoprezygapophyseal lamina (sprl) is oriented anteroposteriorly, while the centroprezygapophyseal lamina (cprl) is oriented dorsoventrally. Between the basis of the prezygapophyses, an intraprezygapophyseal lamina (tprl) is observed, below of which there is the neural canal. To both sides of the neural canal there are the centroprezygapophyseal laminae (cprl). The prezygodiapophyseal lamina (prdl) is well developed and, as the postzygodiapophyseal lamina (podl), is nearly horizontal (Fig. 4B$_1$). The neural spine, although incomplete, is placed nearly at the middle of the vertebra, as in the ~ninth cervical of *D. schrani* (Lacovara et al. 2014: fig. 1A, B), and unlike *P. mayorum*, where it is placed on the posterior half of the vertebra (Carballido et al. 2017: fig. 2a).

Dorsal vertebrae: A posterior (sixth? or seventh?) dorsal vertebra is preserved practically complete (MMCH-Pv 59/3) (Fig. 4C). The centrum is anteroposteriorly short (~220 mm, not counting the condyle), slightly opisthocoelous, and mediolaterally wider (420 mm) than dorsoventrally tall (260 mm) (measurements taken on the posterior cotylus). The deep, subcircular to slightly oval pneumatic fossa is placed on the anterodorsal corner of the lateral face of the centrum, occupying 1/3 of its length. There is not a foramen or small fossa within the pneumatic fossa. Seemingly, its internal structure is solid, without air spaces like camerae or camellae. The ventral face of the centrum is concave anteroposteriorly and lateromedially. This part of the vertebra is broken, so it cannot be known if there was a ventral longitudinal ridge.

The neural arch is vertical and its base occupies the anterior two thirds of the centrum length. In left lateral view (Fig. 4C$_1$), three depressions are observed. The anteriormost is the centroparapophyseal fossa (cpaf, Wilson et al. 2011), which is bounded anteriorly by the anterior centroparapophyseal lamina (acpl), and subdivided by an additional lamina that runs parallel and anteriorly with respect to the acpl. The anterior subfossa is drop-shaped, with its vertex dorsally oriented, whereas the posterior subfossa is placed dorsal and posteriorly with respect to the first one. It is similar to the anterior, but a little larger. It is anteriorly limited by the abovementioned additional lamina and posteriorly by the posterior centroparapophyseal lamina (pcpl). Posteriorly

to the pcpl, there is a fossa located dorsal and posteriorly with respect to the second one. It is triangular, with its vertex ventrally oriented, limited anteriorly by the posterior centroparapophyseal lamina (pcpl), and posteriorly by the posterior centrodiapophyseal lamina (pcdl): this fossa is interpreted as the parapophyseal centrodiapophyseal fossa (pacdf, Wilson et al. 2011).

Posteriorly to the pcdl there is a third, dorsoventrally elongated fossa, which is limited posteriorly by the centropostzygapophyseal lamina (cpol): it is inferred to be the postzygapophyseal centrodiapophyseal fossa (pocdf, Wilson et al. 2011) (Fig. 4C$_1$).

In lateral view, near the base of the neural spine, there is a subcircular fossa interpreted as the postzygapophyseal spinodiapophyseal fossa (posdf), which is anteriorly limited by the posterior spinodiapophyseal lamina (pspdl), ventrally by the postzygodiapophyseal lamina (podl), and posteriorly by the spinopostzygapophyseal lamina (spol) (Fig. 4C$_1$). The hypantrum is formed by two structures, placed one to each side of the midline, which are ventrolaterally projected from the inner corner of the prezygapophyses. Both structures are anteriorly developed, enclosing a deep depression (Fig. 4C$_2$). The prespinal lamina (prsl) is relatively well developed up to the base of the neural spine (Fig. 4C$_2$).

Both rami into which the spinodiapophyseal lamina bifurcates, the anterior (a-spdl) (visible in anterior view, Fig. 4C$_2$) and posterior (p-spdl) rami, are well developed, being parallel one to each other (Fig. 4C$_2$). Between both rami, there is a deep, vertical fossa, the spinodiapophyseal lamina fossa (spdl-f), whose dorsoventral depth varies between 360 mm, medially, and 70 mm, laterally. Although a depression in this place is recorded in other titanosaurs, such as *Epachthosaurus sciuttoi* (Salgado and Powell 2010: fig. 1), *D. schrani* (Voegele et al. 2017, fig. 1), and *Barrosasaurus casamiquelai* (Salgado and Coria 2009: figs. 4, 5), its extreme development and depth is unique in *B. shiva* gen. et sp. nov., by which reason it is considered an autapomorphy of this taxon. The posl, which divides a spof, is poorly developed (Fig. 4C$_3$).

Ventrally to the postzygapophyses, there is an incomplete hyposphene (Fig. 4C$_3$). Although it is very poorly preserved, the hyposphene is as deep as wide (~90 mm). The cpol is double, which makes the cpof to be subdivided.

The neural spine is incompletely preserved, mainly at its tip, but it was apparently undivided, not too high, and vertical. The prespinal lamina is completely formed up to the base of the neural spine (Fig. 4C$_2$). The spol is very poorly preserved (Fig. 4C$_3$).

Caudal vertebrae: Two anterior (MMCH-Pv 59/4, 9th? and MMCH-Pv 59/5, 11th?), one mid (MMCH-Pv 59/6, 16th?), one mid-posterior (MMCH-Pv 59/7, 20th?), and one distal (MMCH-Pv 60/2, 25th?) caudal vertebrae are preserved (Fig. 4E, F; SOM: table 1, Supplementary Online Material available at http://app.pan.pl/SOM/app68-Simon_Salagado_SOM.pdf), as well as two haemal arches (MMCH-Pv 59/8 y MMCH-Pv 59/9).

Anterior caudal vertebrae: The anterior caudal vertebrae of *B. shiva* gen. et sp. nov. are strongly procoelous, with a pronounced condyle placed mostly on the dorsal half of the centrum (Fig. 4E). The internal structure of the anterior caudal vertebrae is solid, like the rest of the caudal vertebrae. The lateral face is slightly concave anteroposteriorly, and almost flat dorsoventrally. In turn, the ventral face is slightly concave anteroposteriorly and relatively flat mediolaterally, which is not flanked by ridges. There is a shallow mid furrow on the posterior half of the ventral face of the centrum, on both sides of which are the articular facets for the haemal arches.

The neural arch is placed on the anterior half of the centrum, as in all titanosaurs, and is somewhat inclined anteriorly. The transverse process is much reduced. In lateral view, the postzygapophysis is ovoid. Below the postzygapophysis is the hyposphene, which is deeper than wide. The neural spine is subrectangular, mediolaterally compressed and vertical (Fig. 4E).

Mid-caudal vertebrae: The centrum of MMCH-Pv 59/6 is high, subcircular in cross-section, and procoelous (Fig. 4F). Its lateral faces are slightly concave anteroposteriorly, and almost flat dorsoventrally, as in the anterior caudals. The ventral face is slightly concave anteroposteriorly and relatively flat laterally and, unlike the anterior caudal, there is no evidence of a mid furrow nor the articular facets for the haemal arches. The base of the neural arch is placed at the anterior half of the centrum. The transverse processes are virtually nonexistent.

Distal caudal vertebrae: MMCH-Pv 60/2 is a badly preserved distal vertebral centrum. It is biconvex, a condition that is present in other titanosaurs such as *Pitekunsaurus macayai* (Filippi and Garrido, 2008) and *Rinconsaurus caudamirus* (Pérez Moreno et al. 2022a) (Fig. 4G).

Haemal arches: Two practically complete haemal arches are preserved: MMCH-Pv 59/8 and MMCH-Pv 59/9 (Fig. 4D). They correspond to the anterior caudals. The anteriormost is more anteroposteriorly expanded at its distal end. The haemal arches are not bridged by bone. The haemal foramen is deep in both arches, extending up to nearly the mid length of the bone, as in *Mendozasaurus neguyelap* (González Riga et al. 2018: fig. 11) and *Baurutitan britoi* (Kellner at al. 2005: figs. 25, 26). The articular facets are flat; there is not a proximal furrow like the observed in *M. neguyelap* (González Riga et al. 2018: fig. 11). The lateral surface of each proximal ramus is flat.

Appendicular skeleton.—Scapular girdle: All the elements of the scapular girdle are preserved: right (MMCH-Pv 59/12) and left (MMCH-Pv 59/13) (Fig. 5A) coracoids; right (MMCH-Pv 59/10) and left (MMCH-Pv 59/11) (Fig. 5B) scapulae; and right (MMCH-Pv 59/14) and left (MMCH-Pv 59/15) (Fig. 5E) sternal plates.

The fact that the coracoid and scapula remain unfused could be indicative of immaturity, as has been postulated in the *D. schrani* type and other sauropods (Lacovara et al. 2014).

Coracoid: The coracoid of *B. shiva* gen. et sp. nov. is rhomboidal, much like that of *P. mayorum* (Carballido et al. 2017: fig. 2p), and different from that of *D. schrani*, where it is subcircular to oval (Lacovara et al. 2014: fig. 2b). The posterior segment of the dorsal margin of the coracoid is level with that of the scapula, as is the case in *D. schrani* (Lacovara et al. 2014: fig. 2b), *P. mayorum* (Carballido et al. 2017: fig. 2p) and other titanosaurs.

The angle between the anterior segment of the dorsal margin and the anterior margin of the coracoid is nearly 105°, whereas that formed by the ventral and anterior margin is nearly 85° (Fig. 5A).

The coracoid becomes progressively thicker downwards, reaching its maximum thickness near its ventral border. The glenoid surface has an infraglenoid lip (Fig. 5A: igl). The coracoid foramen is placed practically on the posterior border of the bone, at the mid-length of the scapular articulation. Finally, the angle between the scapular articulation and the horizontal axis is nearly 50° (Fig. 5A).

Scapula: The scapular proximal lamina forms an angle of nearly 50° with respect to the coracoid articulation, very close to the 45° proposed by Wilson (2002) as a synapomorphy of Nemegtosauridae + ("*Titanosaurus*" *colberti* + Saltasauridae). The glenoid articular surface is subtriangular to semilunar; is anterodorsal-posteroventrally oriented and deviated medially (Fig. 5B).

The anterior fossa is posteriorly limited by a prominent acromial crest, which is originated on the dorsal border: it is ventrally extended forming an angle of nearly 80° with respect to the main axis of the scapula, disappearing towards the area near the ventral border. The region posterior to the acromial crest, the posterior fossa, is concave and short.

The angle between the dorsal margin of the scapular blade and the posterior margin of the acromial process is more than 90°, unlike *D. schrani* (Lacovara et al. 2014: fig. 2) and *M. neguyelap* (González Riga et al. 2018: fig. 12) where this angle is almost 90°, and *P. mayorum*, where it is less than 90° due to the posterior orientation of that process (Carballido et al. 2017: fig. 2). In this regard, the scapula of *B. shiva* gen. et sp. nov. resembles the scapula of the giant titanosaur described by Otero et al. (2021: fig. 3). The acromial crest and the posterior margin of the acromion form an angle of nearly 30°, unlike *D. schrani* (Lacovara et al. 2014: fig. 2) and *M. neguyelap* (González Riga et al. 2018: fig. 12), where they are subparallel. Posterior to the acromial ridge there is a shallow fossa, unlike *M. neguyelap* (González Riga et al. 2018: fig. 12) and *P. mayorum* (Otero et al. 2020: fig. 1B).

The lateral face of the scapular blade is strongly convex and the medial one is flat, which makes the base of the scapular blade D-shaped. On the ventral margin of the bone, at the base of the scapular blade, there is a protuberance or tubercle that is interpreted as the origin of the M. triceps brachii caput scapulocoracoideum, which, according to Otero (2008), is present in a wide array of sauropods, among them species
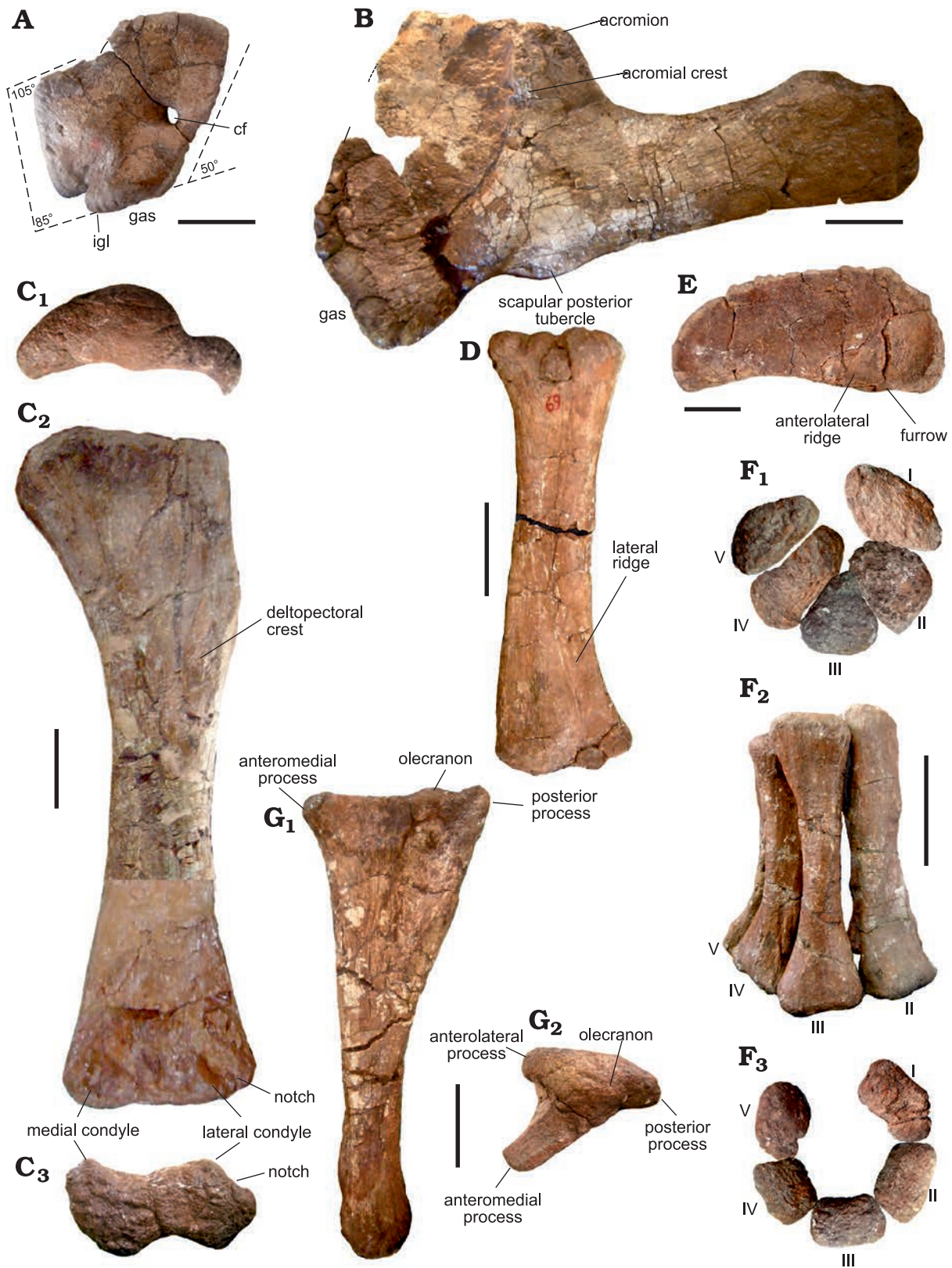
Fig. 5. Forelimb bones of the titanosaurian sauropod *Bustingorrytitan shiva* gen. et sp. nov. from "Bustingorry II" site, Neuquén Province, Argentina, upper Cenomanian. **A**. Left coracoid (holotype, MMCH-Pv 59/13) in lateral view. **B**. Left scapula (holotype, MMCH-Pv 59/11) in lateral view. **C**. Left humerus (holotype, MMCH-Pv 59/21) in proximal (C$_1$), anterior (C$_2$), and distal (C$_3$) views. **D**. Right radius (holotype, MMCH-Pv 59/22) in posterior view. **E**. Left sternal plate (holotype, MMCH-Pv 59/15) in dorsal view. **F**. Articulated metacarpals I–V (holotype, MMCH-Pv 59/25–29) in proximal (F$_1$), anterior (F$_2$) and distal (F$_3$) views. **G**. Right ulna (holotype, MMCH-Pv 59/23) in medial (G$_1$) and proximal (G$_2$) views. Abbreviations: cf, coracoid foramen; gas, glenoid articular surface; igl, infraglenoid lip; I–V, metacarpals. Scale bars 200 mm.

of *Camarasaurus*, *Angolatitan*, *Daxiatitan*, *Chubutisaurus*, *Ligabuesaurus*, and *Elaltitan* (Fig. 5B).

Sternal plate: Both sternal plates are preserved, with the left one (MMCH-Pv 59/15) (Fig. 5E) practically complete, unlike the right one (MMCH-Pv 59/14), which lacks part of its inner portion. The sternal plate is semilunar, being the medial border convex and the lateral one concave in dorsoventral views. It is anteroposteriorly elongate, somewhat wider on the anterior portion than on its posterior portion (Fig. 5E). The anterior, posterior, and medial borders are rugose, while the lateral margin is smooth. On the ventral face, there is an anterolateral ridge, laterally to which there is a furrow (Fig 5E).

Forelimbs: The following elements of the forelimbs are preserved: right and left humeri (holotype); right radius; three ulnae, two from the holotype, and another right element belonging to the smaller paratype. Five complete right metacarpals (holotype), and a metacarpal belonging to the smaller paratype were preserved.

Humerus: In general terms, the humerus of *B. shiva* gen. et sp. nov. is slender, with the right element (MMCH-Pv 59/20) of the holotype a little less slender (Robustness Index = 0.275) than the left one (MMCH-Pv 59/21) (RI = 0.254) (Fig. 5C, SOM: table 2), which is probably due to taphonomical causes. Regarding the average RI (0.2645), the humerus of *B. shiva* gen. et sp. nov. fits within the range from *Rapetosaurus krausei* and *Bonatitan reigi* on one hand (RI = 0.27 Curry Rogers 2009: table 3; Salgado et al. 2014), to on the other hand *Isisaurus* (RI = 0.25, Jain and Bandyopadhyay 1997: table 3) and *Chucarosaurus diripienda* (Agnolin et al. 2023).

The proximal end of the humerus is strongly compressed anteroposteriorly and lateromedially expanded. The dorsal margin is rather straight, at least in its lateral two thirds, unlike *D. schrani* where the dorsal margin is rather subcircular (Lacovara et al. 2014: fig. 2D). In *B. shiva* gen. et sp. nov., the posterior face of the head is strongly convex, forming a subcircular process; this is mostly observed on the left humerus (Fig. 5C$_1$).

The deltopectoral crest is long, anteromedially projected and distally expanded, though not to the extent seen in *D. schrani* (Lacovara et al. 2014: fig. 2D).

On the anterior surface of the proximal third, there is a tuberosity for attachment of the M. coracobrachialis, hardly discernable due to the poor preservation of the bone. The posterior surface of the proximal end is rather flat, and there is not a prominent vertical ridge extending along the lateral margin. On this surface, close to the lateral margin, some below the level of the distal end of the deltopectoral crest, there is the tuberosity for the insertion of the M. latissimus dorsi, which is poorly preserved.

The diaphysis is straight and elliptic in cross-section, with the longitudinal axis transversely oriented. The mediolateral/anteroposterior ratio is 260/110 mm = 2.36 (measurements taken on the holotype MMCH-Pv 59/21).

There is no bulge or tuberosity on the lateral margin of the posterior surface, approximately level with the most prominently developed portion of the deltopectoral crest, which is interpreted as the insertion site for M. scapulohumeralis anterior or M. deltoideus clavicularis in most titanosaurus (Borsuk-Białynicka 1977; Otero 2018; Poropat et al. 2015; Upchurch et al. 2015).

The distal end is less expanded than the proximal one. The medial (ulnar) condyle is a bit more developed anteroposteriorly than the lateral (radial) condyle (Fig. 5C$_2$, C$_3$). The lateral condyle of the humerus is divided on its anterior face by a notch (Fig. 5C$_2$, C$_3$), which is interpreted as an autapomorphy. Between both condyles, no intracondylar crest is observed.

Radius: A right radius is preserved (MMCH-Pv 59/22, holotype). Its length is 970 mm, with a proximal width of 300 mm and distal width of 310 mm; its minimum width at mid diaphysis is 170 mm, and its minimum perimeter is 440 mm (Fig. 5D$_1$). The radius to humerus length ratio is 970/1600 mm = 0.60 and the RI = 0.36. The diaphysis is sigmoid and elliptic in cross section.

On the posterior face, there is the lateral ridge (Fig. 5D$_1$), possibly the interosseous ridge seen in other sauropods such as *P. mayorum* (Otero et al. 2020: fig. 5).

The distal end is expanded and twisted nearly 20° with respect to the longitudinal axis of the diaphysis. There is not a fossa between the condyles.

Ulna: Three ulnae are preserved: two belonging to the holotype (MMCH-Pv 59/23 and MMCH-Pv 59/24, right (Fig. 5G) and left respectively; SOM: table 3), and another right element from the paratype (MMCH-Pv 60/3). The ulnae of the holotype are less robust (right RI = 0.17; left RI = 0.18) than those of the paratype (RI = 0.23). The proximal half of the ulna is triradiate (Fig. 5G$_2$) and its distal half is triangular in cross section. The anteromedial process is much more developed than the lateral process, and the posterior process is moderately developed (Fig. 5G).

The dorsal surface of the anteromedial process is flat and rugose. The olecranon is autapomorphically poorly developed, almost rudimentary, being some lower than the posterior processes (Fig. 5G$_1$).

The medial face of the ulna, strongly concave, is the widest of the three faces of the bone.

The distal end is unexpanded and suboval in cross-section, and has a concavity on its medial face. The articular surface is rugose and convex.

Metacarpus: Five right metacarpals from the holotype are preserved complete (MMCH-Pv 59/25–29; Fig. 5F, SOM: table 4). A metacarpal belonging to the paratype (MMCH-Pv 60/4) is also preserved. All these elements are slender, unlike the only preserved metacarpal of *Chucarosaurus diripienda*, which is robust (Agnolin et al. 2023: fig. 4).

MMCH-Pv 59/25 is a metacarpal I. It is longer than metacarpals IV and V, but shorter than metacarpal II and III. Its proximal articulation has a rough elliptical outline, with the side contacting the metacarpal II being relatively straight, unlike the metacarpal I of *Epachthosaurus sciuttoi*

(Upper Cretaceous, Chubut, Argentina) where the proximal articulation is more triangular (Martínez et al. 2004: fig. 10). The surface of the proximal articulation is slightly convex and rugose. The diaphysis is robust and subelliptic in cross-section. The degree of torsion of the metacarpal I is low, with the angle between the distal and proximal ends being nearly 10°. The triangular articular facet for metacarpal II is placed on the proximal end of the bone, and has small, longitudinal, subparallel ridges. The distal end of metacarpal I, as those of other metacarpals except the V, is trapezoidal in distal view, with the short parallel side oriented internally in the semi-cylinder formed by the five articulated metacarpals.

Metacarpal II (MMCH-Pv 59/26) is, together with metacarpal III, the longest of all. The longest-metacarpal/radius length ratio of *B. shiva* gen. et sp. nov. is 530/970 mm = 0.54, the same value observed in *Epachthosaurus sciuttoi* (297/550 mm, taken on the left forelimb elements, Martinez et al. 2004: tables 2 and 3). The proximal articulation is subtriangular, and its surface is slightly convex and rugose. The diaphysis of metacarpal II is as robust as the diaphysis of the metacarpal I. In cross-section, the diaphysis is subtriangular proximally and subrectangular distally. The degree of torsion of metacarpal II is high, with the angle between the proximal and distal expansions being nearly 90°. As in metacarpal I, the articular facets for other metacarpals are triangular and have longitudinal striations. Particularly, on the distal angle of the articular facet for metacarpal II, there is a protuberance, presumably a ligamentary insertion.

Metacarpal III (MMCH-Pv 59/27) has a degree of torsion of nearly 85°, very similar to that of metacarpal II. Its proximal articulation is an equilateral triangle. As in metacarpal II, the diaphysis is subtriangular proximally and subrectangular distally. The external face in the semi-cylinder formed by the five articulated metacarpals is proximodistally concave and transversely convex.

Metacarpal IV (MMCH-Pv 59/28) is, together metacarpal V, the shortest and most slender of all metacarpals. The degree of torsion is the same as in metacarpal III: 85°. The proximal articulation is subrectangular and elongated. The articular facet for metacarpal V is broad. Distally to this articular facet, there is a protruberance, as in metacarpal II, which is flanked by shallow depressions. The distal end of metacarpal IV is convex and rugose.

Metacarpal V (MMCH-Pv 59/29) is the shortest. The proximal end is D-shaped, as in *Epachthosaurus sciuttoi* (Martínez et al. 2004: fig. 10B), with its convexity externally oriented. Its degree of torsion is relatively low: 30°. In cross-section, the diaphysis is suboval proximally and subcircular distally. The articular facet for metacarpal IV is broad and triangular. Proximally, the articular facet shows the longitudinal striations observed in other metacarpals.

The five metacarpals that form the series would have articulated in a semi-cylindrical arch (Fig. 5F).

Pelvic girdle: All the preserved pelvic elements of *B. shiva* gen. et sp. nov. belong to the holotype: an incomplete left ilium and its pubic peduncle; the pubic peduncle of the right ilium, and the complete right pubis.

Ilium: The element MMCH-Pv 59/16 is an incomplete left ilium, represented by the iliac lamina, mainly its central part, and part of the acetabulum (Fig. 6A). The internal structure of the ilium cannot be established because the ilium is very badly preserved. The anterior sector of the iliac lamina is anteroposteriorly directed. The lateral face of the lamina is anteroposteriorly concave. The medial face, in contrast, is anteroposteriorly convex. The thickness of the ilium increases toward the acetabulum area. The base of the pubic peduncle is wide mediolaterally (235 mm), more than twice its length anteroposteriorly (100 mm). The pubic peduncle has the shape of a truncated cone; its anterior face is convex both proximodistally and mediolaterally, whereas its posterior face, the cotyloid one, is concave in both senses. Only the base of the ischiadic peduncle is preserved.

Pubis: The right pubis (MMCH-Pv 59/19) is preserved (Fig. 6B) except for the ischiadic peduncle and the area surrounding the pubic foramen. The articulation for the ilium is relatively horizontal in lateromedial view and establishes an angle of nearly 145° with the acetabular portion, which is incompletely preserved. The articulation for the ilium is strongly expanded anteroposteriorly. The pubic lamina is plate-like, and has its distal end slightly expanded anteroposteriorly.

Hindlimbs: Four incomplete femora from different individuals are preserved; three tibiae from different individuals, two incomplete and one complete; two incomplete fibulae; two astragali from different individuals; three metatarsals; and three ungual phalanges.

Femora: Four incomplete femora of different sizes are preserved (right MMCH-Pv 59/30, holotype, Fig. 6E; right MMCH-Pv 60/5, paratype, Fig. 6F; MMCH-Pv 61/1 and MMCH-Pv 62/1; SOM: table 5).

Although the Robustness Index could not be estimated in any of the specimens due to their incompletness, the femur is an apparently robust bone.

The right femur of the holotype (MMCH-Pv 59/30) preserves its proximal end and part of its diaphysis (Fig. 6E). On the lateral border, below the greater trochanter, there is the typical lateral bulge of the titanosauriforms (Salgado et al. 1997). In this respect, the *B. shiva* gen. et sp. nov. femur is very different from that of *Chucarosaurus diripienda*, which is characterized by having a straight lateral edge (Agnolin et al. 2023: fig. 7). On the posterolateral surface of the proximal portion of the femur, there is a poorly developed longitudinal ridge, even less developed than that observed in *P. mayorum* (Otero et al. 2020: fig. 8B, L), which is interpreted as a relictual trochanteric shelf. The diaphysis, at the proximal end, is anteroposteriorly compressed, presenting a subelliptical cross-section, with the greater axis lateromedially oriented. On the posterior face, on the medial border, there is a prominent fourth trochanter.

The preserved femur of the paratype MMCH-Pv 60/5 corresponds to the distal extremity and part of the diaphysis
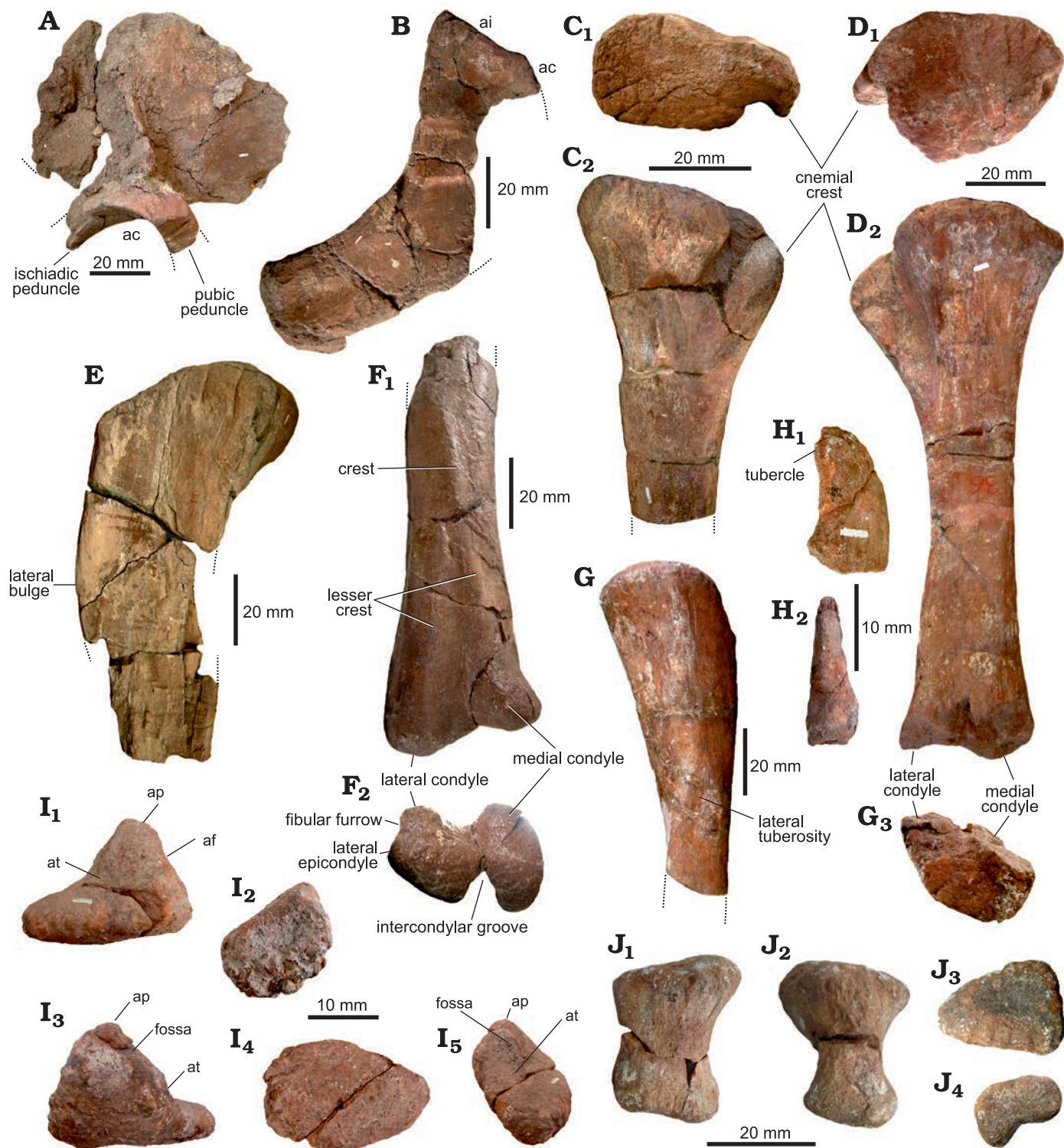
Fig. 6. Pelvic and hindlimb elements of the titanosaurian sauropod *Bustingorrytitan shiva* gen. et sp. nov. from "Bustingorry II" site, upper Cenomanian. **A**. Right ilium (holotype, MMCH-Pv 59/16) in medial view. **B**. Right pubis (holotype, MMCH.Pv 59/19) in medial view. **C**. Proximal portion of right tibia (holotype, MMCH-Pv 59/31) in proximal (C_1) and lateral (C_2) views. **D**. Left tibia (paratype, MMCH-Pv 60/6) in proximal (D_1), lateral (D_2), and distal (D_3) views. **E**. Proximal portion of right femur (holotype, MMCH-Pv 59/30) in anterior view. **F**. Distal portion of right femur (paratype, MMCH-Pv 60/5) in anterior (F_1) and distal (F_2) views. **G**. Proximal portion of right fibula (holotype, MMCH-Pv 59/32) in lateral view. **H**. Right phalange ungual II (holotype, MMCH-Pv 59/39) in lateral (reversed) (H_1) and plantar (H_2) views. **I**. Left astragalus (holotype, MMCH-Pv 59/34) in anterior (I_1), lateral (I_2), posterior (I_3), distal (I_4), and medial (I_5) views. **J**. Left metatarsal I (holotype, MMCH-Pv 59/35) in dorsal (J_1), medial (J_2), proximal (J_3) and distal (J_4) views. Abbreviations: ac, acetabulum; af, articulation for the fibula; ai, articulation for the ilium; ap, ascending process; at, articulation for the tibia.

of a right element (Fig. 6F). This bone, as MMCH-Pv 59/30, seems to be robust. On the anterior face of the diaphysis, there is a low and angled crest, which runs proximodistally, and is absent in *Chucarosaurus diripienda* (Agnolin et al. 2023: fig. 7). This crest is interpreted as the linea intermuscularis cranialis, seen in some titanosaurs such as *Neuquensaurus australis* (Otero 2010: fig. $10A_1$ and A_2). As in *Neuquensaurus australis* (Otero 2010), this crest seems to bifurcate distally into two lesser crests, each one being directed to one or other of the condyles. The medial (tibial) and lateral (fibular) condyles are prominent. The medial condyle is more anteroposteriorly developed, but the lateral condyle extends further distally with respect to the other (Fig. $6F_2$). Between both condyles, there is a deep intercondylar groove, absent in *Chucarosaurus diripienda* (Agnolin et al. 2023: fig. 7). In turn, between the fibular condyle and the lateral epicondyle, there is a shallow fibular furrow (Fig. 6F).

The element MMCH-Pv 61/1 corresponds to an almost complete, although badly preserved, left femur. The piece MMCH-Pv 62/1 corresponds to a fragment of the distal end of a right femur. Due to the poor preservation of these elements, the description of the femur was based on the type material and the MMCH-Pv 60/5.

Fibulae: Both the right (MMCH-Pv 59/32) (Fig. 6G) and left (MMCH-Pv 59/33) fibulae of the holotype are preserved, albeit incomplete. The fibula seems to be relatively slender (as there are no complete elements, it is not possible to know its RI). The medial face of the bone is flat to slightly concave; however, on its proximal sector, it is strongly concave due to the presence of the tibial mark. The lateral tuberosity is well developed, although it is not flanked by ridges (Fig. 6G). The piece is not complete enough to know if it has an anterolateral triochanter, such as the present in *M. neguyelap* (González Riga et al. 2018: fig. 20O).

Tibiae: The tibia of *B. shiva* gen. et sp. nov. is known based on three elements: an incomplete right tibia, which is part of the holotype (MMCH-Pv 59/31, Fig. 6C), and two left tibiae, one belonging to the paratype (MMCH-Pv 60/6, Fig. 6D), and the other to one of the referred specimens (MMCH-Pv 62/2, SOM: table 6).

The proximal end of the tibia of the holotype (MMCH-Pv 59/31) is subrectangular in proximal view, with its greater axis anteroposteriorly oriented (Fig. $6C_1$).

The left tibia of the paratype (MMCH-Pv 60/6) is complete (Fig. 6D). The bone is slender (RI = 0.263), fitting within the range recorded in *Bonatitan mayorum* (RI = 0.266 and 0.257, Salgado et al. 2014), but less slender than in *Laplatasaurus araukanicus* (RI = 0.22, Gallina and Otero 2015). The proximal half of this tibia is similar to that of the holotype; however, its proximal extremity is suboval in cross-section (Fig. $6D_1$). The cnemial crest is subtriangular and there is not a tuberculum fibularis on its posterior surface, as is present in some titanosauriforms and flagellicaudatans (Mannion et al. 2017).

In turn, the distal end is somewhat anteroposteriorly expanded, unlike *Chucarosaurus diripienda* where it is

clearly unexpanded (Agnolin et al. 2023: fig. 8). The medial condyle extends slightly more ventrally than the lateral condyle (Fig. $6D_2$). The tibia of the MMCH-Pv 62/2 consists of a distal extremity and part of a diaphysis of a left element.

Astragali: Two left astragali are preserved: that of the holotype (MMCH-Pv 59/34, Fig. 6I), and that of MMCH-Pv 62/3.

The astragalus is wedge-shaped. The ascending process is high; the articulation for the tibia broad, and the articulation for the fibula is concave and faces laterally. A shallow fossa is observed in medial view; it seems to be single, undivided. No foramina are observed at the base of the ascending process.

The element MMCH-Pv 59/34 has been associated with the holotype because of its size. Its anteroposterior length (190 mm) is 76% of the lateromedial (transversal) length (250 mm). On the other hand, its lateromedial (transversal) length is greater than 50% of its proximodistal height (120 mm) (Wilson 2002: ch. 214). Specifically, the lateromedial length represents 208% of the proximodistal heigth.

The element MMCH-Pv 62/3 is greater than MMCH-Pv 59/34. The anteroposterior length (180 mm) is 60% of the lateromedial length (300 mm). On the other hand, the lateromedial length is greater than 50% of the proximodistal height (140 mm). Specifically, the lateromedial length represents 214% of the proximodistal height.

Metatarsals: Three metatarsals are preserved (MMCH-Pv 59/35–37, holotype). MMCH-Pv 59/35 corresponds to the left metatarsal I (Fig. 6J, SOM: table 7). It is the most robust and the shortest of the recovered metatarsals. The greater axis of the distal end is rotated 50° with relation to the major axis of the proximal end. On the other hand, the distal end has two condyles, one of them, whose position is plantar lateral (posterolateral), is more distally projected than the other one, a character formerly interpreted as a synapomorphy of flagellicaudatan diplodocoids (Wilson 2002: ch. 220).

MMCH-Pv 59/36 is an incomplete metatarsal, probably the IV. It is more slender than the metatarsal I. Evidently, both the proximal and distal ends of the bone were expanded.

MMCH-Pv 59/37 is a right metatarsal V. This bone is paddle-shaped, characterized by its great lateromedial compression and the superoplantar expansion.

Ungual phalanges: Three right ungual phalanges of the holotype are preserved, MMCH-Pv 59/38, 39 (Fig. 6H), and MMCH-Pv 59/40, corresponding respectively to digits I, II, and III. These bones are lateromedially compressed and superoplantarly expanded. The dorsal border is convex and the ventral border is strongly concave.

The proximal end has a soboval to romboidal articular surface, with the greater diameter vertically oriented, and the lesser diameter lateromedially oriented. The distal end of the unguals is pointed, although in the three preserved elements the tip is not preserved. On the ventral face of unguals I and II there seems to be a ridge-like tubercle towards the distal end (Fig. $6H_1$), such as the present one in *M. neguye-*

lap (González Riga et al. 2018: fig. 24) and a wide array of titanosauriforms.

The lateral face is proximodistally and superoplantarly convex; in turn, the medial face is flattened proximodistally and superoplantarly.

The largest ungual phalange is the first, and the smallest one is the third (SOM: table 8). The phalanx of ungual I is nearly 25% longer than the phalanx of ungual III.

Body mass estimation

Undoubtedly, *Bustingorrytitan shiva* gen. et sp. nov. was a huge sauropod, comparable in size to the largest sauropods recorded to date. The gigantic titanosaurs recorded in Patagonia cover a temporal range from late Early Cretaceous (*Patagotitan mayorum*) to Late Cretaceous (*Puertasaurus reuili*, *Dreadnoughtus schrani*) (Otero et al. 2021), *B. shiva* gen. et sp. nov. (as well as the fragmentary *Chucarosaurus diripienda*, Agnolin et al. 2023) falls halfway between those two points.

The methods for estimating body mass are many, and the results are not always coincident when distinct methods are employed (Campione and Evans 2012: table 6). For the calculation of body mass, the formula of Campione and Evans (2012) can be used for quadrupedal tetrapods, for which it is necessary to know the minimum circumference of femur and humerus. The formula is as follows:

$$\text{Log BM} = 2.749 \times \log (\text{CH+CF}) - 1.104$$

where CH is the minimum circumference of the humerus and CF the minimum circumference of the femur.

The minimum circumference of the femur of *B. shiva* gen. et sp. nov. is (MMCH-Pv 59/30) is 760 mm (reconstructed) (Simón, 2011), and the minimum perimeter of the humerus (MMCH-Pv 59/20) is 680 mm.

$$\text{Log BM} = 2.749 \times \log (76+68) - 1.104$$
$$2.749 \times 2.158 - 1.104$$
$$4.828$$
$$\text{BM} = 67.297 \text{ tons}$$

Applying a mean PPE of 25.6% (Campione and Evans 2012), results in an estimated body mass of *B. shiva* gen. et sp. nov. between 50.069 and 84.525 tons (±17.228 of standard error).

Taking into account the caveat that the minimum circumference of the femur is reconstructed, the body mass value obtained for *B. shiva* gen. et sp. nov. is greater than the 59.3 metric tons calculated for *D. schrani* (Lacovara et al. 2014), and not much less than the 69 tons calculated for *P. mayorum* (Carballido et al. 2017). It should be remembered that the holotype of *B. shiva* gen. et sp. nov. (MMCH-Pv 59) is somewhat smaller than one of the MMCH-Pv 62, which would agree with the idea that the holotype does not correspond to a fully-grown animal. A complete paleohistological analysis of the specimen could shed light on the ontogenetic stage of these specimens.

Phylogenetic analysis

To evaluate the phylogenetic position of *Bustingorrytutan shiva* gen. et sp. nov. amongst 103 sauropodormphs, we used the data matrix of Pérez Moreno et al. (2022b), which in turn is a modified version of the data matrix of Gallina et al. (2021) (see SOM). The data matrix was analyzed with TNT v.1.6 (Goloboff and Morales 2023). The search strategy consisted of a combination of algorithms including Wagner trees, TBR branch swapping and sectorial search until 100hits (command "xmult=hits100"). A second TBR search was carried out with the aim of expanding the tree space; as a result, 999.999 MPT of 1639 steps were obtained (CI = 0.326; RI = 0.704).

Node support for MPTs was calculated using Bootstrap, Jacknife and Bremer. Bootstrap values were 57 or higher across all macronarian nodes, and those of Jacknife were 73 for the macronians; 64 for *Europasaurus* plus the others above, and 57 for all others (all excluding *Europasaurus*). In turn, Bremer support was calculated using the TNT script bremsup.run that combines heuristic searches of suboptimal trees allied to tree searches under negative constraints (Bremer values higher than 1 are indicated in Fig. 7).

The strict consensus tree revealed several polytomies, one of which consisted of all lithostrotians except *Malawisaurus* (Lithostrotia = *Malawisaurus* + *Saltasaurus*), which was placed as the sister taxon of all other lithostrotians: precisely, within this polytomy nested *B. shiva* gen. et sp. nov. To identify the taxa causing the polytomies, we applied the Iter PCR command. Thus, the following unstable macronarians were identified: *Isanosaurus*, *Andesaurus*, *Malarguesaurus*, *Lusotiutan*, *Sauroposeidon*, *Abydosaurus*, *Brachiosaurus*, *Epachthosaurus*, *Puertasaurus*, *Tapuiasaurus*, *Nemegtosaurus*, and *Rayososaurus*. Once we pruned these taxa with the pruntax command, the internal nodes to Lithostrotia were resolved, and the number of trees was reduced to 4139 (Fig. 7).

The strict reduced consensus recovered *B. shiva* gen. et sp. nov. as a saltasauroid (*Saltasaurus*, not *Patagotitan*), the sister group of Saltasauridae (*Opisthocoelicaudia* + *Saltasaurus*) (Fig. 7), with which it shares characters 232, 287, 290, and 350. Saltasauridae, in turn, share the following characters, not observed in *Bustingorrytitan*: 236, 276, 297, 303, and 377 (see SOM). The analysis revealed a series of 29 autapomorphic characters for *B. shiva* gen. et sp. nov. (those indicated with an asterisk in the diagnosis).

The analysis failed to recover the Titanosauria (*Andesaurus* + *Saltasaurus*), because *Andesaurus* (one of the specifiers of the clade) had to be pruned because of its unstability. In Fig. 7 Titanosauria is labeled with an interrogative sign taking into account the alternative position of *Andesaurus* in the cladogram that best fits with the phylogenetic definition of the clade.

The analysis also did not resolve the polytomy at the base of Eutitanosauria (*Patagotitan* + *Saltasaurus*), which implies that some of the taxa could be left out of Eutitanosauria. All phylogenetic definitions are from Carballido et al. 2022.

Fig. 7. Strict consensus of the phylogenetic analysis, after pruning the unstable taxa, showing the different alternative positions of *Andesaurus* (asterisk). Bremer support values higher than 1 are shown. Note: to save space only the part of the cladogram from *Patagosaurus* onwards is shown.

Discussion

Gigantic titanosaurs were an important component of the Cretaceous dinosaur faunas of Patagonia, at least for almost 50 million years. The finding of *Bustingorrytitan shiva* gen. et sp. nov. increases our knowledge of these extraordinary animals, not only in terms of their anatomical diversity but also their evolutionary history.

The lithostrotian condition of *B. shiva* gen. et sp. nov. revealed by the phylogenetic analysis presented in this work, supports the coexistence of at least two lineages of gigantic titanosaurs (saltasauroids and lognkosaurs) within the same area (North Patagonia), at the same time (early Late Cretaceous).

The early Late Cretaceous is a particularly important time for the evolutionary history of sauropods, both globally and regionally. Particularly, the time represented by the base of the Huincul Formation (late Cenomanian) is relevant for its diversity of sauropods: mid to large-sized titanosaurs (like *Choconsaurus baileywillisi*, Simon et al. 2018), small to mid-sized basal diplodocoids (Simón and Salgado 2009), and gigantic titanosaurs such as *B. shiva* gen. et sp. nov. Following Otero et al. (2021), the sauropod diversity in the Cenomanian–Turonian interval in the Neuquén Basin, expressed not only in terms of body size but also in terms of dental morphology, may have been possible by a process of niche partitioning.

Towards the Cenomanian–Turonian boundary, a global faunal turnover marked the extinction of basal diplodocoids and of certain lineages of titanosaurs, as well as of other dinosaur groups (Coria and Salgado 2005). However, some saltasauroid and lognkosaur lineages exceeded that limit, surviving until practically the end of the Cretaceous. Among the latter are the gigantic titanosaurs, such as *Notocolossus gonzalezparejasi*.

So far, latest Cretaceous gigantic titanosaurs are limited to southern Patagonia. Although northern Patagonia has been explored more extensively and for much longer, no gigantic titanosaurs have been recorded. Of course, this hypothesis could be discarded with new findings, but a local extinction of gigantic titanosaurs from northern Patagonia in pre-Campanian times should not be ruled out.

Conclusions

A new gigantic titanosaur, *Bustingorrytitan shiva* gen. et sp. nov., is recorded. It comes from the same stratigraphic unit as the basal colossosaur *Chucarosaurus diripienda* and the lognkosaur *Argentinosaurus huniculensis*, the first gigantic titanosaur to be described. *Bustingorrytitan shiva* gen. et sp. nov. exhibits a series of diagnostic characters, among them posterior dorsal vertebrae with spinodiapophyseal lamina bifurcated in two, very well developed anterior (aspdl) and posterior (pspdl) rami, which limit a deep, vertical, socket-et-like fossa; posterior dorsal neural arches with forked centropostzygapophyseal laminae (cpol); hyposphene in anterior

caudal vertebrae; humerus with deltopectoral crest strongly expanded distally; and femur with a low longitudinal crest on the lateromedial half of the anterior face, bifurcated in two minor crests, which are directed to their respective condyles. *Bustingorrytitan shiva* gen. et sp. nov. has an estimated body mass of 67.297 metric tons (with a standard error of ±17.228), which makes it one of the largests sauropods ever recorded. The phylogenetic analysis performed recovers *B. shiva* gen. et sp. nov. as a derived lithostrotian, the sister group of Saltasauridae. The existence of gigantic lithostrotians corroborates that gigantism (evolutions of forms over the 50 metric tones) would have evolved many times within Eutitanosauria.

Acknowledgements

References

Agnolin, F.L., González Riga, B.J., Aranciaga Rolando, A.M., Rozadilla, S., Motta, M.J., Chimento, N.R. and Novas, F.E. 2023. A new giant titanosaur (Dinosauria, Sauropoda) from the Upper Cretaceous of Northwestern Patagonia, Argentina. *Cretaceous Research* 146: 105487.

Anderson, J.F. 1985. Long-bone circumference and weight in mammals, birds and dinosaurs. *Journal of the Zoological Society of London A* 207: 53–61.

Bonaparte, J.F. and Coria, R.A. 1993. Un Nuevo y gigantesco saurópodo titanosaurio de la Formación Río Limay (Albiano-Cenomaniano) de la Provincia del Neuquén, Argentina. *Ameghiniana* 30: 271–282.

Bonaparte, J.F. and Powell, J.E. 1980. A continental assemblage of tetrapods from the Upper Cretaceous beds of El Brete, northwestern Argentina (Sauropoda-Coelurosauria-Carnosauria-Aves). *Mémoires De La Société Géologique De France* 139: 19–28.

Borsuk-Białynicka, M. 1977. A new camarasaurid sauropod *Opisthocoelicaudia skarzynskii* gen. n., sp. n. from the Upper Cretaceous of Mongolia. *Palaeontologia Polonica* 37: 1–64.

Calvo, J.O. 1994. Jaw mechanics in sauropod dinosaurs. *Gaia* 10: 183–193.

Calvo, J.O. 2014. New fossil remains of *Futalognkosaurus dukei* (Sauropoda, Titanosauria) from the Late Cretaceous of Nequén, Argentina. *In*: C.V. Rubinstein, C.A. Marsicano, and B.G. Waisfeld (eds.), *Fourth International Paleontological Congress Meeting, Mendoza, Argentina, 28 September 2014–3 October 2014*, 325. Mendoza.

Calvo, J.O., Porfiri, J.D., González Riga, B.J., and Kellner, A.W.A. 2007. A new Cretaceous terrestrial ecosystem from Gondwana with the description of a new sauropod dinosaur. *Anais da Academia Brasileira de Ciências* 79: 529–541.

Campione, N.E. and Evans, D.C. 2012. A universal scaling relationship between body mass and proximal limb bone dimensions in quadrupedal terrestrial tetrapods. *BMC Biology* 10 (1): 60.

Carballido, J.L., Otero, A., Mannion, P.D., Salgado, L., and Moreno, A.P. 2022. Titanosauria: A critical reappraisal of its systematics and the relevance of the South American record. *In*: A. Otero, J.L. Carballido, and D. Pol (eds.), *South American Sauropodomorph Dinosaurs*, 269–298. Springer Earth System Sciences, Berlin.

Carballido, J.L., Pol, D., Otero, A., Cerda, I.A., Salgado, L., Garrido, A.C., Ramezani, J., Cúneo, N.R., and Krause, J.M. 2017. A new giant titanosaur sheds light on body mass evolution among sauropod dinosaurs. *Proceeding of the Royal Society B* 284: 20171219.

Coria, R.A. and Salgado, L. 2005. Mid-Cretaceous turnover of saurischian communities: evidence from the Neuquén Basin, *In*: G. Veiga, L. Spalletti, J.A. Howell, and E. Schwartz (eds.), The Neuquén Basin: A Case Study in Sequence Stratigraphy and Basin Dynamics. *Special Publications of the Geological Society* 252: 317–327.

Curry Rogers, K. 2009. The postcranial osteology of *Rapetosaurus krausei* (Sauropoda: Titanosauria) from the Late Cretaceous of Madagascar. *Journal of Vertebrate Paleontology* 29: 1046–1086.

Filippi, L.S. and Garrido, A.C. 2008. *Pitekunsaurus macayai* gen. et sp. nov., nuevo titanosaurio (Saurischia, Sauropoda) del Cretácico Superior de la Cuenca neuquina, Argentina. *Ameghiniana* 45: 575–590.

Gallina, P.A. and Otero, A. 2015. Reassessment of *Laplatasaurus araukanicus* (Sauropoda: Titanosauria) from the Upper Cretaceous of Patagonia, Argentina. *Ameghiniana* 52: 487–501.

Gallina, P.A., Canale, J.I., and Carballido, J.L. 2021. The earliest known titanosaur sauropod dinosaur. *Ameghiniana* 58: 35–31.

Goloboff, P.A. and Morales, M. 2023. TNT version 1.6, with a graphical interface for MacOs and Linux, including new routines in parallel. *Cladistics* 39 (2): 144–153.

González Riga, B.J., Lamanna, M.C., Ortiz, D.L.D., Calvo, J.O., and Coria, J.P. 2016. A gigantic new dinosaur from Argentina and the evolution of the sauropod hind foot. *Scientific Reports* 6: 19165.

González Riga, B.J., Mannion, P.D., Poropat, S.F., Ortiz David, L.D., and Coria, J.P. 2018. Osteology of the Late Cretaceous Argentinean sauropod dinosaur *Mendozasaurus neguyelap*: implications for basal titanosaur relationships. *Zoological Journal of the Linnean Society* 184: 136–181.

Jain, S.L. and Bandyopadhyay, S. 1997. New titanosaurid (Dinosauria: Sauropoda) from the Late Cretaceous of central India. *Journal of Vertebrate Paleontology* 17: 114–136.

Kellner, A.W.A., Campos, D.A., and Trotta, M.N.F. 2005. Description of a titanosaurid caudal series from the Bauru Group, Late Cretaceous of Brazil. *Arquivos do Museu Nacional* 63: 529–564.

Lacovara, K.J., Lamanna, M.C., Ibiricu. L.M., Poole, J.C., Schroeter, E.R., Ullmann, P.V., Voegele, K.K., Boles, Z.M., Carter, A.M., Fowler, E.K., Egerton, V.M., Moyer, A.E., Coughenour, C.L., Schein, J.P., Harris, J.D., Martínez, R.D., and Novas, F.E. 2014. A gigantic, exceptionally complete titanosaurian sauropod dinosaur from Southern Patagonia, Argentina. *Scientific Reports* 4: 6196.

Mannion, P.D., Allain, R., and Moine, O. 2017. The earliest known titanosauriform sauropod dinosaur and the evolution of Brachiosauridae. *PeerJ* 5:e3217.

Martínez, R.D., Giménez, O., Rodríguez, J., Luna, M., and Lamanna, M.C. 2004. An articulated specimen of the basal titanosaurian (Dinosauria: Sauropoda) *Epachthosaurus sciuttoi* from the early Late Cretaceous Bajo Barreal Formation of Chubut Province, Argentina. *Journal of Vertebrate Paleontology* 24: 107–120.

Novas, F.E., Agnolín, F., Rozadilla, S., Aranciaga-Rolando, A., Brisson-Egli, F., Motta, M., Cerroni, M., Ezcurra, M., Martinelli, A., D´Angelo, J., Álvarez-Herrera, G., Gentil, A., Bogan, S., Chimento, N., García Marsá, J., Lo Coco, G., Miquel, S., Brito, F., Vera, E., Pérez Loinaze, V., Fernández, M., and Salgado, L. 2019. Paleontological discoveries in the Chorrillo Formation (upper Campanian–lower Maastrichtian, Upper Cretaceous), Santa Cruz Province, Patagonia, Argentina. *Revista del Museo Argentino de Ciencias Naturales* 21: 217–293.

Novas, F.E., Salgado, L., Calvo, J.O., and Agnolín, F. 2005. Giant titanosaur (Dinosauria, Sauropoda) from the Late Cretaceous of Patagonia. *Revista del Museo Argentino de Ciencias Naturales* 7: 37–41.

Otero, A. 2018. Forelimb musculature and osteological correlates in Sauropodomorpha (Dinosauria, Saurischia). *PLoS ONE* 13 (7): e0198988.

Otero, A., Canale, J.I., Haluza, A., and Calvo, J.O. 2011. New titanosaur with unusual haemal arches from the Upper Cretaceous of Neuquén Province, Argentina. *Ameghiniana* 48: 655–661.

Otero, A., Carballido, J.L., and Pérez Moreno, A. 2020. The appendicular osteology of *Patagotitan mayorum* (Dinosauria, Sauropoda), *Journal of Vertebrate Paleontology* 40 (4): e1793158.

Otero, A., Carballido, J.L., Salgado, L., Canudo, J.I., and Garrido, C.A. 2021. Report of a giant titanosaur sauropod from the Upper Cretaceous of Neuquén Province, Argentina. *Cretaceous Research* 122: 104754.

Pérez Moreno, A.N., Carballido, J.L., Otero, A., Salgado, L., and Calvo, J.O. 2022a. The axial skeleton of *Rinconsaurus caudamirus* (Sauropoda: Titanosauria) from the Late Cretaceous of Patagonia, Argentina. *Ameghiniana* 59: 1–46.

Pérez Moreno, A.N., Otero, A., Carballido, J.L., Salgado, L., and Calvo, J.O. 2022b. The apendicular skeleton of *Rinconsaurus caudamirus* (Sauropoda: Titanosauria) from the Upper Cretaceous of Patagonia, Argentina. *Cretaceous Research* 142: 105389.

Poropat, S.F., Mannion, P.D., Upchurch, P., Hocknull S.A., Kear B.P., and Elliott, D.A. 2015. Reassessment of the non-titanosaurian somphospondylan *Wintonotitan wattsi* (Dinosauria: Sauropoda: Titanosauriformes) from the mid-Cretaceous Winton Formation, Queensland, Australia. *Papers in Palaeontology* 1: 59–106.

Salgado, L. and Coria, R.A. 2009. *Barrosasaurus casamiquelai* gen. et sp. nov., a new titanosaur (Dinosauria, Sauropoda) from the Anacleto Formation (Late Cretaceous: early Campanian) of Sierra Barrosa (Neuquén, Argentina). *Zootaxa* 2222: 1–16.

Salgado, L. and Powell, J.E. 2010. Reassessment of the vertebral laminae in some South American titanosaurian sauropods. *Journal of Vertebrate Paleontology* 30: 1760–1772.

Salgado, L., Coria, R.A., and Calvo. J.O. 1997. Evolution of titanosaurid sauropods I: phylogenetic analysis based on the postcranial evidence. *Ameghiniana* 34: 3–32.

Salgado, L., Gallina, P.A., and Paulina Carabajal, A. 2014. Redescription of *Bonatitan reigi* (Sauropoda: Titanosauria), from the Campanian–Maastrichtian of the Río Negro Province (Argentina). *Historical Biology* 27: 525–548.

Simón, M.E. 2011. *Los dinosaurios saurópodos de la Formación Huincul (Cenomaniano superior) en Villa El Chocón (Neuquén): osteología, relaciones filogenéticas, aspectos paleoecológicos, y paleobiogeográficos.* 493 pp. Unpublished Thesis, Facultad de Ciencias Exactas, Físicas y Naturales, Universidad Nacional de Córdoba, Córdoba.

Simón, M.E. and Salgado, L. 2009. New materials of Diplodocoidea (Sauropoda) from Villa El Chocón, Huincul Formation (Cenomanian– early Turonian), Neuquén Province, Argentina. *In*: *Resúmenes de las XIV Jornadas Argentinas de Paleontología de Vertebrados, May 4–7, 2009*, 56. San Rafael (Mendoza).

Simón, M.E., Salgado, L., and Calvo, J.O. 2018. A new titanosaur sauropod from the Upper Cretaceous of Patagonia, Neuquén Province, Argentina. *Ameghiniana* 55: 1–29.

Upchurch, P., Barrett, P.M., and Dodson, P. 2004. Sauropoda. *In*: D.B. Weishampel, P. Dodson, and H. Osmólska (eds.), *The Dinosauria*, *2nd edition*, 259–322. University of California Press, Berkeley.

Upchurch, P., Mannion P.D., and Taylor M.P. 2015. The anatomy and phylogenetic relationships of "*Pelorosaurus*" *becklesii* (Neosauropoda, Macronaria) from the Early Cretaceous of England. *PLoS ONE* 10: e0125819.

Voegele, K.K., Lamanna, M.C., and Lacovara, K.J. 2017. Osteology of the dorsal vertebrae of the giant titanosaurian sauropod dinosaur *Dreadnoughtus schrani* from the Late Cretaceous of Argentina. *Acta Palaeontologica Polonica* 62: 667–681.

Wilson, J.A. 2002. Sauropod dinosaur phylogeny: critique and cladistics analysis. *Zoological Journal of the Linnean Society* 136: 215–275.

Wilson, J.A., D'Emic, M.D., Ikejiri, T., Moacdieh, E.M., and Whitlock J.A. 2011. A nomenclature for vertebral fossae in sauropods and other saurischian dinosaurs. *PLoS One* 6 (2): e17114.